Nanocharacterization by TEM and AFM

We offer a wide range of TEM and AFM tools, from TEM grids and finders to AFM substrates and grippers.

Available in a wide variety of designs and materials to support your work, select from a broad range of mesh sizes, specimen supporting films, and materials that perfectly suit the conditions of your TEM analysis.

TEM grid specifications:

Material	Mesh Size and Shape	Film Specifications
• Cu • Ni • Au • Mo • Cu/Pd	• Square or hexagonal • Single-hole grid (75 mm or 100 mm) • 100 • 150 • 200 • 300 • 400	• None • Continuous formvar film (thicknesses: 5-6 nm, 10 nm) • Lacey carbon film (average hole sizes: 50 nm, 100 nm, 150 nm, 100 mm, 150 mm) • Continuous amorphous carbon film (thicknesses: 10 nm, 20-30 nm) • Continuous formvar/ carbon film (thickness: 10nm formvar and 1nm carbon)

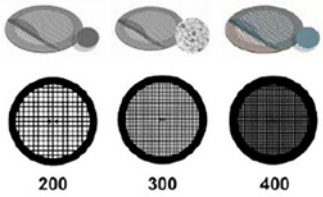

TEM finder grid specifications:

Material	Mesh Size	Film Specifications
• Cu • Ni • Au	• 135 • 200 • 300 • 400	• None • Continuous amorphous carbon film (thicknesses: 3-4 nm, 10 nm, 20-30 nm)

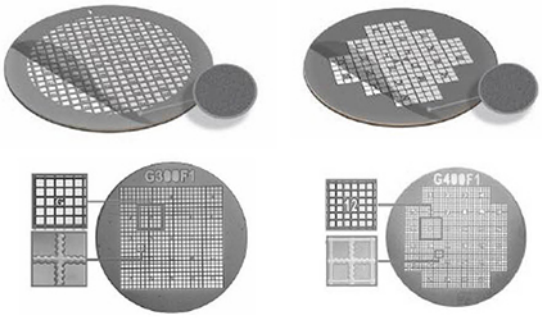

Supporting Tools for Nanomaterial Characterization

Our comprehensive range of supporting materials for nanomaterial characterization includes tweezers (sharp tip, disc gripper for AFM), TEM window grids (various thicknesses, 1 or 9 windows), a magnetic pick-up tool, a grid storage box, cryo-capsules, lift-out grids (Cu or Mo), AFM substrates (various dimensions), and much more.

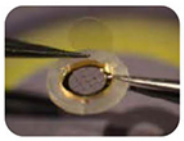

Explore our complete range of TEM grids on:
SigmaAldrich.com/nanocharacterization

© 2022 Merck KGaA, Darmstadt, Germany and/or its affiliates. All Rights Reserved. Merck, the vibrant M, and Sigma-Aldrich are trademarks of Merck KGaA, Darmstadt, Germany or its affiliates. All other trademarks are the property of their respective owners. Detailed information on trademarks is available via publicly accessible resources.

MK_AD9792EN 43729 08/2022

The Life Science business of Merck operates as MilliporeSigma in the U.S. and Canada.

Sigma-Aldrich®
Lab & Production Materials

Check for updates

Energy Technology
Generation, Conversion, Storage, Distribution
www.entechnol.de

21944296, 0, Downloaded from https://onlinelibrary.wiley.com/doi/10.1002/ente.202200859 by Karlsruher Inst F. Technologie, Wiley Online Library on [11/10/2022]. See the Terms and Conditions (https://onlinelibrary.wiley.com/terms-and-conditions) on Wiley Online Library for rules of use; OA articles are governed by the applicable Creative Commons License

Experimental Investigation of the Temperature, Pressure, and Binder System Influence on Vacuum Postdrying Processes and Moisture Management of Li-Ion Battery Electrodes

Thilo Heckmann, Jochen Christoph Eser, Andreas Altvater, Natalie Streller, Philip Scharfer, and Wilhelm Schabel*

Moisture management and postdrying are crucial for Li-ion battery lifetime and performance as well as overall energy efficiency of electrode production. An optimization of these processes by a fundamental comprehension of sorption and mass transport mechanisms in the electrode holds potential to increase sustainability of this technology. The composition of electrodes determines which of these mechanisms govern the interaction of electrodes with water from atmosphere. In this study, the influence of the binder system, temperature, and pressure of Li-ion battery anodes on postdrying is focused on. Anodes with the binder system carboxymethylcellulose (CMC)/styrene–butadiene–rubber (SBR) and polyvinylidene fluoride represent a mostly absorbing and mostly adsorbing material system, respectively. Variation of the process parameters temperature and pressure reveals that both material systems show a similar impact of pressure on water mass transport in the electrode during water removal, although a reduced pressure impact for the CMC/SBR system is expected, since in this case most water is absorbed into the polymers and should diffuse independently of the system pressure. Temperature affects water mass transport in the absorbing material system stronger than in the adsorbing material system, due to the strong temperature dependency of the water diffusion inside the absorbing polymers.

1. Introduction

The production of state-of-the-art battery electrodes comprises several sequential process steps.[1–4] These process steps mutually affect each other and largely contribute to the battery's properties and performance.[5–8] Accompanying these process steps, the moisture management of an electrode production chain is responsible for the final water content in the cell.[2] This final water content may detrimentally influence a battery's performance and lifetime.[5,9,10] The moisture management envelopes the monitoring and regulation of sorption and desorption processes along the production chain of battery electrodes. From an economical point of view, this management requires a large share of the energy demand of the electrode production chain.[11] Therefore, it is advisable to optimize the moisture management and with it the postdrying process during cell production, which increases sustainability of batteries by decreasing the energy demand of battery production. This optimization necessitates a fundamental comprehension of the phenomena that govern sorption and desorption processes along the process chain and, especially, the phenomena during postdrying.

As a crucial part of the moisture management, this postdrying initiates a final desorption process prior to cell assembly.[2] The postdrying removes residual water that absorbs into electrode and separator materials during preceding process steps.[5,6,12–15] This final desorption prior to cell assembly can be vastly accelerated and controlled by postdrying compared with desorption at dry-room conditions. Key elements to this acceleration are temperature, dew-point temperature, pressure, and the distance a molecule must travel to desorb from a battery component (compare **Figure 1**).[6,12]

At process level, this distance refers to half the width of an electrode in a coil. The desorption process combines ab- and adsorption and mass transport phenomena in multiple components including porous media and polymer binders.[13,14] The widely utilized vacuum batch postdrying is also affected by mass transport at low pressure, which includes the transition through several diffusion regimes.[16] Notably, these fundamentally different mass transport mechanisms respond individually to system parameters (e.g., temperature, pressure). Furthermore,

T. Heckmann, J. C. Eser, A. Altvater, N. Streller, P. Scharfer, W. Schabel
Thin Film Technology (TFT)
Karlsruhe Institute of Technology (KIT)
76131 Karlsruhe, Germany
E-mail: thilo.heckmann@kit.edu

The ORCID identification number(s) for the author(s) of this article can be found under https://doi.org/10.1002/ente.202200859.

© 2022 The Authors. Energy Technology published by Wiley-VCH GmbH. This is an open access article under the terms of the Creative Commons Attribution License, which permits use, distribution and reproduction in any medium, provided the original work is properly cited.

DOI: 10.1002/ente.202200859

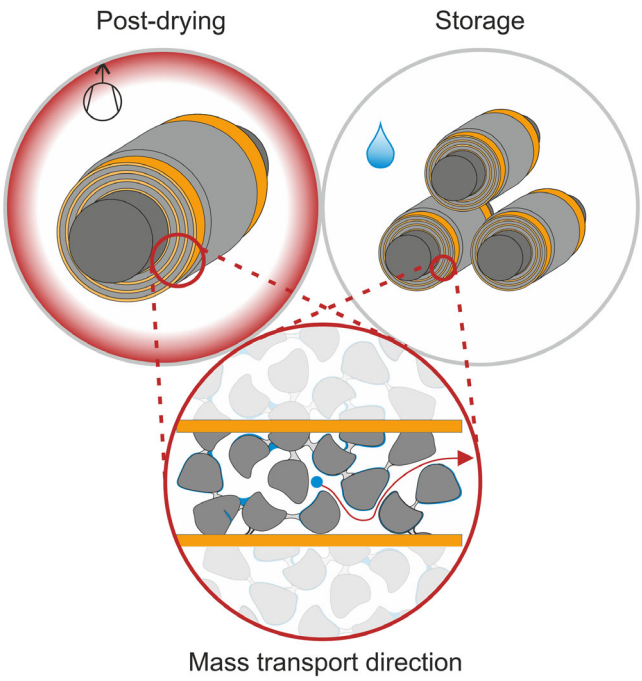

Figure 1. Illustration of the similarity of postdrying and storage of electrode coils regarding mass transport. Both processes can be abstracted by a 1D mass transport direction in axial to the coil. This abstraction is also valid for storage and postdrying of pouch and cylindrical cells prior to electrolyte filling.

depending on these parameters, the various mass transport mechanisms can have a major or minor impact on the overall kinetics of the process. The vacuum postdrying combines all these elements and will therefore be subject of this study. The comprehension of the physical phenomena behind the acceleration of the desorption is crucial for the component-specific optimization of the drying process.

Many authors address moisture management and postdrying during the production of battery electrodes. Eser et al. studied the general sorption behavior of anodes and showed that sorption equilibria of anodes can be assembled with slight deviations by adding up the sorption equilibria of its individual components.[14] Furthermore, Eser et al. showed that some materials of a battery electrode express a hysteresis in their sorption behavior, which emphasizes the importance of postdrying.[13] Li et al. investigated the moisture content of NMC532 cathode as a function of postdrying temperature and processing.[17] Sicklinger et al. showed that nickel-containing cathode active materials (CAM) are prone to surface contamination due to water in the atmosphere.[18] Schuer et al. found proof for chemically bound water to the surface of the particles of CAM and their detrimental effect on electrochemical performance.[10] Huttner et al. concluded that regardless of the chemical sorption in cathodes, the water sorption is also a function of the surface available for water molecules to attach.[15] These studies provide copious insight into equilibrium states and do not quantify kinetic phenomena during sorption.

Postdrying routines are mentioned in several studies, which have been reviewed by Huttner et al.[6] This summary revealed a large diversity of postdrying routines and, therefore, emphasizes the significance of a fundamental understanding for this process. Huttner et al. developed a universally applicable postdrying routine in a vacuum oven that proofed to be a feasible method for cathode, anode, and separator.[6] In addition, Huttner et al. showed that process conditions (e.g., temperature and duration) of postdrying affect cell performance and lifetime of Li-ion batteries.[5] Eser et al. considered mass transport in the polymers carboxymethyl cellulose (CMC) and styrene–butadiene–rubber (SBR), which allows conclusion on the drying mechanisms that govern postdrying.[12] These studies provide insight into vacuum postdrying routines and their effect on cell performance and also on the drying kinetics in binder polymers. However, kinetic investigations of vacuum postdrying are unavailable. These kinetic investigations are necessary to fundamentally understand the physical processes during desorption.

This study provides time-resolved drying curves of Li-ion battery anodes in coil geometry that resemble industrial process conditions and provide a defined mass transport distance. Furthermore, the influence of the system parameters temperature and pressure, as well as the binder system on the desorption during postdrying and moisture management, is investigated. The different dependencies of various mass transport phenomena inside an electrode on the system parameters provide insight into relevant mass transport resistances. The results are applicable to moisture management as well as postdrying at low pressure.

2. Results and Discussion

Initially, a comparison of the sorption behavior of two electrodes shows the dominant sorption mechanism. This comparison is based on literature data and own experiments. The anode's active material, graphite, physically adsorbs water on its surface.[14] The cathode's active material, for example, lithium–nickel–manganese–cobalt oxides exhibits a complex interaction with water that combines chemical and physical sorption.[18–20] In this study, the focus lies on two common binders, applied to Li-ion battery anodes, to show the influence of the binder system on postdrying and moisture management. One electrode is an anode with a PVDF–NMP (polyvinylidene fluoride, N-methyl-2-pyrrolidone) binder system and the other one is an anode with a CMC/SBR–water binder system. The anodes contain graphite as active material. Both binder systems are applicable to anode and cathode, although aqueous processing for cathodes is challenging and the subject of current studies.[21–23]

Drying experiments at various pressure settings and temperatures elucidate the significance of individual sorption mechanisms of the two electrodes. In addition, mass transport mechanisms that can occur due to system parameters (pressure and temperature) are discussed. The results allow first conclusions about which mass transport phenomena are relevant for moisture management and postdrying.

2.1. Influence of the Binder System on Water Sorption of Electrodes

The composition of an electrode determines the mechanisms that govern the water uptake during electrode production. The active materials constitute the largest weight proportion of an

© 2022 The Authors. Energy Technology published by Wiley-VCH GmbH

21944296, 0, Downloaded from https://onlinelibrary.wiley.com/doi/10.1002/ente.202200859 by Karlsruher Inst F. Technologie, Wiley Online Library on [11/10/2022]. See the Terms and Conditions (https://onlinelibrary.wiley.com/terms-and-conditions) on Wiley Online Library for rules of use; OA articles are governed by the applicable Creative Commons License

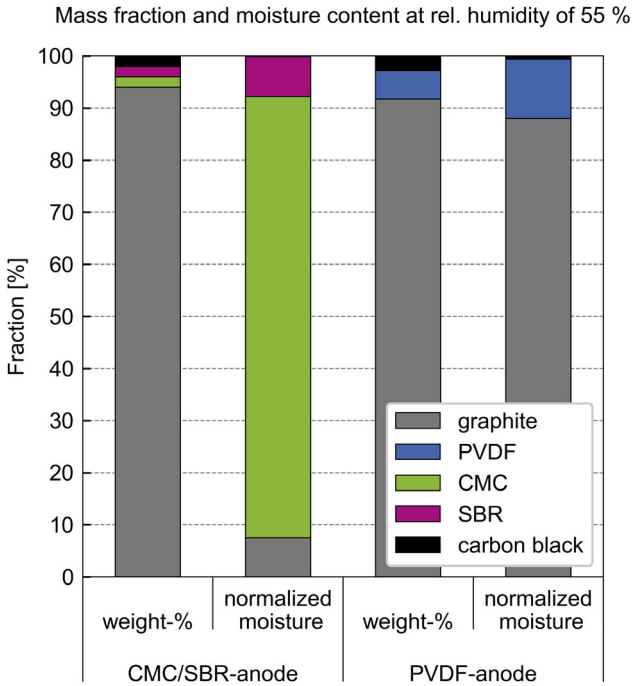

Figure 2. Bar chart of the component proportion and moisture content for the CMC/SBR anode and PVDF anode.[13,14] The first bars of each anode show the composition of the respective anode in weight percent. The second bars plot the water content of each component of the anodes normalized to the anode's entire water content. Colors indicate the component of the individual anode. The moisture content of the individual components relates to a relative humidity of 55%.

electrode; nevertheless, the additives can significantly contribute to the moisture uptake of an electrode (compare **Figure 2**).[14] The binder system CMC/SBR leads to a mostly absorbing electrode, with most of the water being absorbed into the polymeric CMC and SBR binder. Using the binder PVDF leads to a mostly adsorbing electrode, with most of the water being adsorbed on the surface of the active material graphite.

Figure 2 plots the component composition of the CMC/SBR anode and the PVDF anode in weight percent. In addition, the water content of the individual components is scaled to 100 weight percent of the entire water content of the respective anode. The comparison of the water content in the components takes place at a relative humidity of 55%, which is the starting condition for all drying experiments in this study. The sorption data of the individual components is obtained from literature and listed in the supporting information.[14]

The CMC/SBR anode consists of 94 wt% graphite and 2 wt% each CMC, SBR, and carbon black. The mass fraction of the graphite is large compared with the other components. However, 85% of the water that is absorbed by this anode rests in the 2 wt% CMC binder. The 2 wt% SBR takes up about 7% of the totally absorbed water equivalent to graphite. The water adsorbed by carbon black is insignificant compared with the other components. The binders CMC and SBR absorb water and express an internal diffusion resistance.[12] Thus, 92% of the water content in the CMC/SBR anode is absorbed into the polymeric binders, representing the absorbing material system.

The PVDF anode consists of 91.7 wt% graphite, 5.5 wt% PVDF, and 2.8 wt% carbon black. In this case, the water loading of the graphite poses 88% of the absorbed water of the entire PVDF anode. According to Eser et al., graphite adsorbs water to its surface.[13,14] The water content of the carbon black makes up less than 1% and the water content of the PVDF makes up 11% of the PVDF anode's water content. The sorption equilibrium of PVDF and water is listed in supporting information (Figure S1). The exact sorption mechanism of PVDF is unknown and an absorbing sorption behavior cannot be ruled out. However, 89% of the water in the PVDF anode is adsorbed on graphite and carbon black. Under this circumstance, the PVDF anode represents the adsorbing material system, compared with the CMC/SBR anode.

Temperature and pressure affect these sorption mechanisms and mass transport of the model electrodes differently. The mass transport through the porous structure is susceptible to changes in pressure if it is governed by diffusion.[16,24–26] In addition, convection affects the mass transport at a pressure close to the vapor pressure of water. The diffusion coefficient of water in a polymeric binder, for example, CMC, is greatly affected by the temperature and unaffected by pressure.[12] These circumstances will be exploited to identify governing mass transport resistances during postdrying by systematically changing the system parameters.

2.2. Adsorbing Material System: Influence of Temperature and Pressure

The PVDF anode poses the adsorbing material system. Therefore, dominant mass transport resistance during the drying of this anode is expected to be mass transport through the gas phase inside the coil geometry. Which gas phase mass transport mechanisms prevail, depends on the temperature and pressure conditions.

2.2.1. Drying Curves at Low Temperature

The drying curves of the adsorbing anode at 30 °C are expected to be predominantly governed by diffusional mass transport through the gas phase. Nevertheless, the water content of the PVDF binder could desorb at a slower rate than the adsorbed water and, therefore, result in a slower drying toward lower water loadings of the PVDF anode. **Figure 3** shows the drying curves of the adsorbing anode at 30 °C and different system pressures.

Figure 3 plots the water loading of the anode in parts per million on the y-axis versus the time in hours on the x-axis. The x-axis plots values from −0.1 to 5 h. The experimental data prior to 0 h are the equilibrium with a relative humidity 55% and 0 h marks the initiation of the drying experiment. The markers show the drying curves at the individual system pressures. The cell is continuously purged with dry nitrogen to avoid a saturated gas phase above the sample.

The PVDF anode dries slowest at 800 mbar. A pressure reduction from 800 to 400 mbar (factor 2) accelerates drying by a similar increment as the pressure reduces from 400 to 100 mbar (factor 4). The drying curves at 40 and 20 mbar, inducing a reduction by the factor of 2.5 and 5 compared with the drying curve

© 2022 The Authors. Energy Technology published by Wiley-VCH GmbH

21944296, 0, Downloaded from https://onlinelibrary.wiley.com/doi/10.1002/ente.202200859 by Karlsruher Inst F. Technologie, Wiley Online Library on [11/10/2022]. See the Terms and Conditions (https://onlinelibrary.wiley.com/terms-and-conditions) on Wiley Online Library for rules of use; OA articles are governed by the applicable Creative Commons License

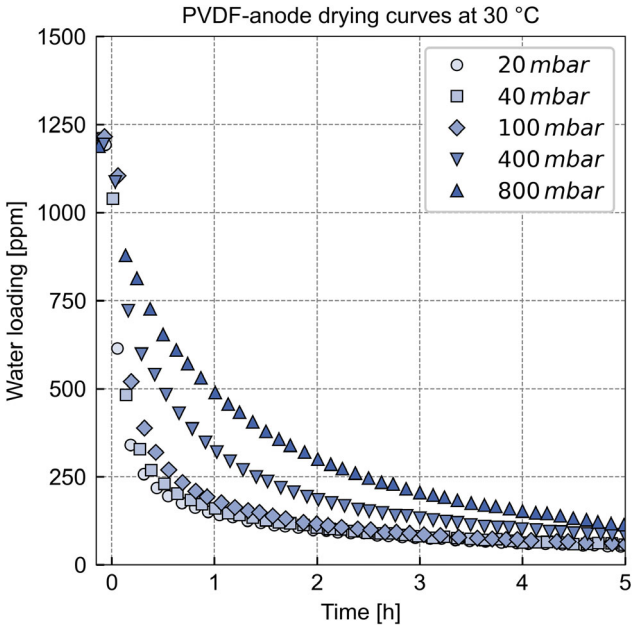

Figure 3. Drying curves at different pressures for an electrode with a mostly adsorbing sorption mechanism (PVDF anode) with a porosity of 35% at a temperature of 30 °C.

of 100 mbar, do not accelerate significantly. This shows that the efficiency of pressure reduction, regarding the desorption speed, depends on the absolute pressure levels.

This observation can be explained by the pressure dependency of the gas-phase diffusion coefficient in a porous structure. Depending on the pressure and pore diameter, the diffusion regime in the gas phase of a porous structure changes from the Stefan regime (continuum) to the Knudsen regime (discontinuum) when lowering the system pressure.[16] This change of diffusion regimes from Stefan to Knudsen results in a decreasing pressure dependency until the diffusion coefficient in the Knudsen regime is not a function of the system pressure anymore.

Gaps between individual layers of the electrode could occur, even by tightly wounding the coil during sample preparation. These gaps would accelerate the mass transport inside the electrode coil as mass transport trough these gaps is not restricted by the porous structure. Therefore, gaps would be beneficial regarding the drying time and need to be considered during evaluation of the experiments.

In addition, convective transport can affect the mass transport through the electrode coil. Convective transport occurs as the pressure decreases toward the vapor pressure of water at 30 °C (compare Figure S2, Supporting Information). If the system pressure approaches the vapor pressure at a given temperature, the molar fraction of water in the gas phase of the electrode rises. If the concentration is sufficiently large, drag fluxes occur in addition to the diffusion, accelerating the process. Figure S2, Supporting Information, shows that this phenomenon affects the 40 and 100 mbar drying curves. Furthermore, a reduction of the system pressure below the vapor pressure can induce a pressure-driven convection until the sorption equilibrium adjusts between sample and gas phase, which could be the case for the 20 mbar drying curve.

The drying experiments were carried out until no significant mass change over several hours was detected, which indicates that the sample reached the sorption equilibrium with the dry nitrogen flow and serves as the criterion for the end of drying. The data are plotted over the course of 5 h to emphasize the differences of the drying curves. However, the drying curves converge after 5 h of drying time. This circumstance indicates that an additional mass transfer resistance governs the drying of the remaining water that is not susceptible to pressure. Therefore, an additional mass transport resistance, for example, diffusion resistance in a component of the PVDF anode, is expected to be the cause of slow drying at the low water loadings of the samples.

2.2.2. Drying Curves at High Temperature

A temperature increase affects the gas-phase diffusion coefficient and accelerates the diffusion in the continuum as well as in the discontinuum. The transition between continuum and discontinuum is also a function of temperature. However, the influence of the temperature on this transition is insignificant in the considered temperature range. Thus, the pressure dependency of the diffusion coefficient remains similar as for the diffusion coefficient at 30 °C. The temperature affects the vapor pressure of water exponentially, increasing the volatility of water at all pressure levels and therefore an additional acceleration due to convection is expected.

The results of the drying experiments at various pressures at a temperature of 80 °C are plotted in **Figure 4**.

In Figure 4, again the water loading of the drying anode is plotted over time for the adsorbing anode at 80 °C. Compared

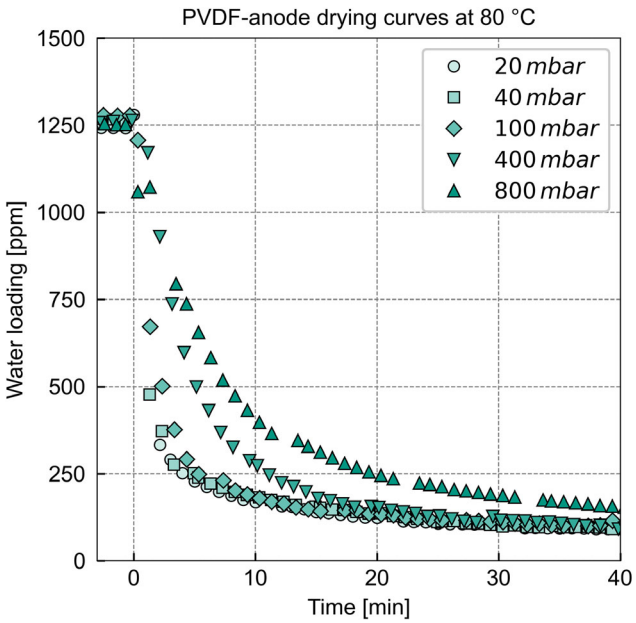

Figure 4. Drying curves at different pressures for an electrode with a mostly adsorbing sorption mechanism (PVDF anode) with a porosity of 35% at a temperature of 80 °C.

© 2022 The Authors. Energy Technology published by Wiley-VCH GmbH

21944296, 0, Downloaded from https://onlinelibrary.wiley.com/doi/10.1002/ente.202200859 by Karlsruher Inst F. Technologie, Wiley Online Library on [11/10/2022]. See the Terms and Conditions (https://onlinelibrary.wiley.com/terms-and-conditions) on Wiley Online Library for rules of use; OA articles are governed by the applicable Creative Commons License

with Figure 3, which shows the results for the adsorbing electrode at 30 °C, the scale of the x-axis shows only 40 min of drying time instead of 5 h. The occurring interruptions between several markers result from the tarring of the balance to avoid incorrect measurement data due to a signal drift. These interruptions are insignificant for larger timescales, for example, in Figure 3.

As expected, increasing the drying temperature decreases the drying time for all pressure levels. The drying curves transition into the pressure-independent slow drying (compare PVDF anode at 30 °C) after ≈40 min as opposed to 5 h at 30 °C.

The acceleration of drying due to pressure reduction seems to follow a similar trend as for 30 °C—the influence of pressure is also less pronounced toward the pressure reduction below 100 mbar.

The vapor pressure of water surpasses or is in the same order of magnitude as the drying pressure in the measurement cell for the experiments at 80 °C (compare Figure S2, Supporting Information). These pressure conditions suggest that convection accelerates the mass transport inside the electrode.

The slow drying at low water loadings of the coils occurs for all pressure levels. However, this slow drying occurs sooner compared with the drying curves at 30 °C. In addition, the drying curves reach the criterion for the end of drying sooner than the drying curves at 30 °C. Therefore, the resistance responsible for the slow drying at low water loadings is reduced by an increase in temperature.

2.2.3. Comparison of Drying Curves at Different Temperatures

A side-by-side comparison of the drying curves at different temperatures allows an analysis of the temperature influence on the drying of mostly adsorbing anodes. The drying curves for the lowest and the highest pressure considered in this study will be compared with each other, because the difference of the temperature influence on the gas-phase diffusion coefficient is most pronounced at these pressure levels. In addition, the magnitudes of the influence of the convective fluxes due to the water concentration in the gas phase will be most pronounced at these pressures. If this phenomenon occurs and affects drying, a larger acceleration of the drying experiments from 30 to 80 °C is expected compared with the increase solely attributed to the temperature dependency of the diffusion coefficient of water in the gas phase. The difference in drying times, observed experimentally between 30 and 80 °C, is illustrated in **Figure 5**.

Figure 5 plots the drying curves at 20 and 800 mbar for 30 and 80 °C. Both plots show the water loading over time. The equilibrium water loading at 30 °C is 50 ppm lower than at 80 °C. This difference can be attributed to a temperature-dependent sorption behavior.

Regardless of the larger initial solvent loading of the PVDF anode at 80 °C compared with the initial solvent loading at 30 °C, the drying accelerates at both pressure levels. This finding can be explained by the temperature dependencies of the gas-phase diffusion coefficient (continuum $\approx T^{1.75}$, discontinuum $\approx T^{0.5}$).[27,28] Furthermore, convection is a function of the vapor pressure of water, which expresses an exponential dependency of the temperature. The temperature appears to have a stronger influence on the desorption at 800 mbar compared with 20 mbar. This could be due to stronger temperature influence on the diffusion coefficient of the continuum diffusion. However, a precise differentiation between these mechanisms as well as a quantification of the temperature influence requires a simulation that considers gas-phase diffusion and convection, which is beyond the scope of this study.

The consideration of the system parameters temperature and pressure and the analysis of the drying curves suggest that gas-phase diffusion through a porous structure as well as convection pose the mass transport through the mostly adsorbing electrode coil. In addition, a pressure-independent resistance governs the drying at very low water loadings.

2.3. Absorbing Material System: Influence of Temperature and Pressure

The CMC binder contains most of the water that absorbs to an anode with the CMC/SBR binder system (compare Figure 2). During the sorption of water in CMC, the water absorbs into the volume of the polymer. Depending on the process

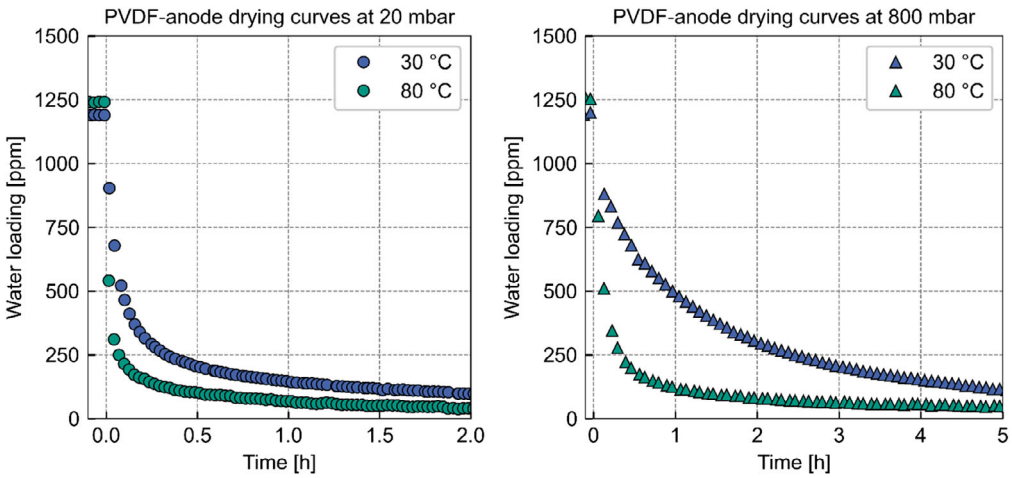

Figure 5. Influence of the postdrying temperature at 20 and 800 mbar on the drying of an electrode with a mostly adsorbing binder system (PVDF anode).

© 2022 The Authors. Energy Technology published by Wiley-VCH GmbH

21944296, 0, Downloaded from https://onlinelibrary.wiley.com/doi/10.1002/ente.202200859 by Karlsruher Inst F. Technologie, Wiley Online Library on [11/10/2022]. See the Terms and Conditions (https://onlinelibrary.wiley.com/terms-and-conditions) on Wiley Online Library for rules of use; OA articles are governed by the applicable Creative Commons License

parameters of postdrying and the geometry of the polymer in the electrode, this sorption may pose an additional mass transport resistance that needs to be considered when postdrying CMC/SBR anodes.[12] However, if this mass transport affects the postdrying process, depending on the transport distance, the water must travel through the polymer until it can desorb into the surrounding gas phase. This transport distance is unknown, as the exact geometrical configuration of the polymers inside an electrode is intricate to determine.[29,30] A variation of the process parameters will indicate which mass transport mechanisms affect the postdrying of an absorbing material system, based on their individual dependencies.

2.3.1. Drying Curves at Low Temperature

The diffusion coefficients of water in CMC and SBR vary across two orders of magnitude in the temperature range from 30 to 80 °C.[12] Therefore, the influence of the polymer diffusion on the drying of the CMC/SBR anodes is expected to be most significant at 30 °C, as the diffusion coefficient of water in CMC is extremely low at such low temperatures. Pressure does not influence the diffusion in polymers.[12] Thus, if pressure does not affect the drying of a CMC/SBR anode, only the diffusion of water in the polymers governs drying. If pressure affects the drying, the mass transport through the porous gas phase also affects drying. **Figure 6** presents drying curves at 30 °C and different system pressures.

Figure 6 shows the water loading of the CMC/SBR anode during drying over time. The markers show the drying curves for three different pressures. The timescale of these drying experiments is comparatively large (<60 h). Therefore, the number of drying experiments of the CMC/SBR anode at 30 °C was limited to three pressures: 20, 100, and 800 mbar. The CMC/SBR anode absorbs more water than the PVDF anode. This increase can be attributed to the strongly sorbing CMC binder (compare Figure 2). The duration of drying indicates that the polymer sorption affects the drying significantly. Remarkably, although most of the water is absorbed in the polymer, pressure influences drying. The drying curves express pressure dependency like the mostly adsorbing PVDF anode does. This observation indicates that the gas-phase mass transport affects the drying of the absorbing anode, even though most of the water is absorbed in the binder and must diffuse through the binder prior to traveling through the gas phase.

Another similarity to the drying experiments of the adsorbing anode at 30 °C (see Figure 3) is the slow drying at low water loadings after a certain period. The diffusion in the polymeric binders is expected to cause this slow drying, which becomes speed limiting toward the end of the drying. The fact that diffusion in the polymer binder decelerates as the water loading in the polymer sinks further supports this hypothesis.

2.3.2. Rying Curves at High Temperature

When increasing the drying temperature to 80 °C, a significant decrease of the drying time is expected as the desorption of the water absorbed by the polymeric binders occurs faster compared with the experiment at 30 °C. The gas-phase diffusion is expected to affect drying as well because the accelerated polymer diffusion will increase the amount of water that must be transported through the gas-phase per time. Thus, the drying of the CMC/SBR-anode at higher temperature is expected to be affected by both mass transport mechanisms. **Figure 7** plots the drying curves of the CMC/SBR anode at 80 °C and different system pressures.

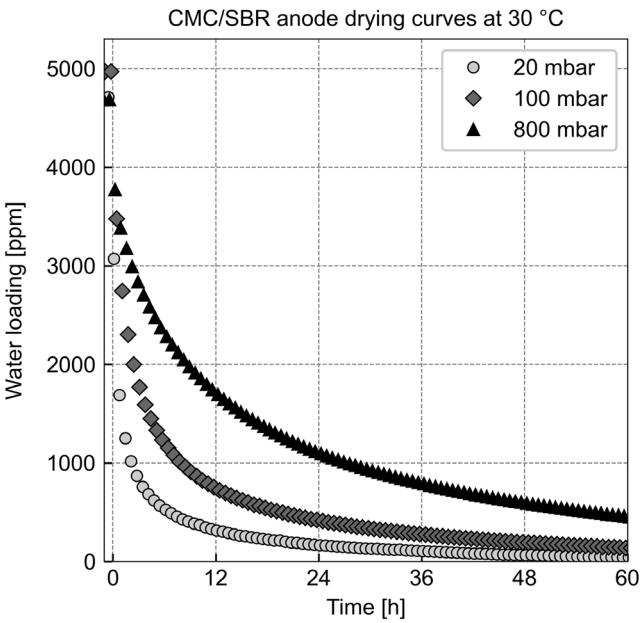

Figure 6. Drying curves at different pressures for an electrode with a mostly absorbing sorption mechanism (CMC/SBR anode) with a porosity of 35% at 30 °C.

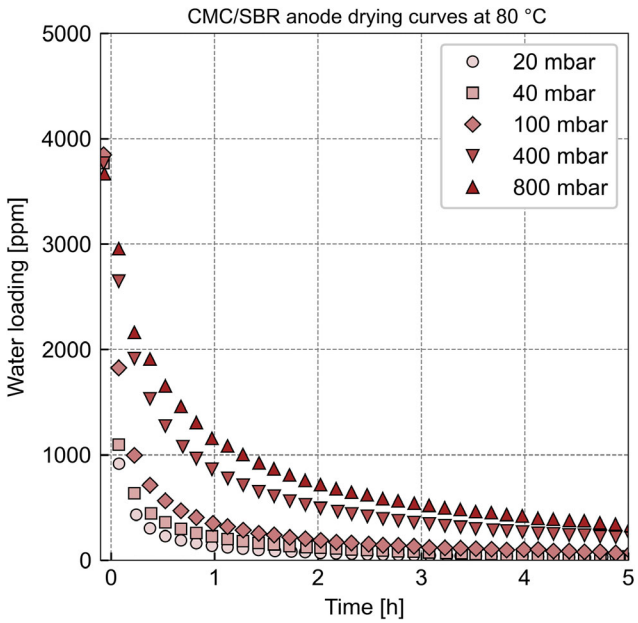

Figure 7. Drying curves at different pressures for an electrode with a mostly absorbing sorption mechanism (CMC/SBR anode) with a porosity of 35% at a temperature of 80 °C.

© 2022 The Authors. Energy Technology published by Wiley-VCH GmbH

21944296, 0, Downloaded from https://onlinelibrary.wiley.com/doi/10.1002/ente.202200859 by Karlsruher Inst F. Technologie, Wiley Online Library on [11/10/2022]. See the Terms and Conditions (https://onlinelibrary.wiley.com/terms-and-conditions) on Wiley Online Library for rules of use; OA articles are governed by the applicable Creative Commons License

Figure 7 shows the drying curves of the CMC/SBR anode as water loading plotted over time. The equilibrium water loadings of the CMC/SBR anode differ by 1000 ppm from 30 to 80 °C for a relative humidity of 55%. The sorption equilibria of the binders CMC and SBR have a temperature dependency, which explains the deviation of the measured equilibrium loadings. Eser et al. showed that water loading of polymers decreases with increasing temperature.[13] This temperature effect on the equilibrium loading of the CMC/SBR anode is the opposite of the observation of the PVDF anode.

The vast decrease in drying time compared with the experiments at 30 °C indicates that the mass transport resistance in the polymer binders significantly contributes to the overall resistance of the CMC/SBR anode. However, a simulation of the polymer desorption coupled with the mass transport through the gas phase of the electrode is necessary to quantitatively confirm this hypothesis. The pressure dependency of the drying curves shows that the mass transport through the gas phase of the electrode also affects drying, similar to the pressure dependency of the PVDF anode.

3. Conclusion

This study presents a method to conduct time-resolved desorption experiments for the postdrying and moisture management of battery electrode production. The setup allows the gravimetric measurement of samples that resemble electrode coils with a defined mass transport direction in the axial direction of the coil at various pressure conditions. Prior to the desorption, the sorption equilibrium at a defined relative humidity is adjusted in the sample. Dry nitrogen constantly purges the measurement cell to ensure dry boundary conditions for the desorption.

3.1. Binder System

Anodes with a water-based CMC/SBR and NMP-based PVDF binder system represent a mostly absorbing and mostly adsorbing electrode, respectively. CMC/SBR anodes absorb larger quantities of water compared with the mostly adsorbing PVDF anodes, which originates in the sorption behavior of the CMC/SBR binder systems. Apart from the gas-phase mass transport in the porous structure, both anodes express an additional mass transport resistance that could be attributed to adsorption kinetics in the graphite or polymer diffusion in the polymeric binder.

3.2. Pressure

A decrease in pressure accelerates the desorption of both anodes. The influence of the pressure reduction on the process acceleration depends on the absolute pressures and decreases toward lower pressures. This observation indicates that the diffusion through the porous structure affects the mass transport. In addition, the combination of the system parameters temperature and pressure also determines whether convection accelerates the gas-phase mass transport through the coil. The pressure dependency occurs regardless of the different governing sorption mechanisms in the CMC/SBR anode and PVDF anode. Thus, the desorption of water out of the volume of the CMC binder does not solely dominate the mass transport through the CMC/SBR coils.

3.3. Temperature

The CMC/SBR anode desorbs on a different timescale compared with the PVDF anode, which shows the necessity of high temperatures during postdrying. A temperature increase accelerates the desorption of the CMC/SBR and PVDF anode. This acceleration appears to be more pronounced for the CMC/SBR anode than for the PVDF anode, which could be caused by the large temperature dependency of the polymer diffusion of the absorbed water in the CMC binder.

A precise quantification of the observed temperature dependency of the CMC/SBR anode requires further experiments and a comparative simulation. In the simulation, multiple mass transport phenomena, for example, polymer drying and gas-phase diffusion, have to be coupled to elucidate the governing mass transport resistances as a function of system parameters which will be addressed in subsequent studies.

In short, this experimental study provides time-resolved desorption experiments of Li-ion battery anodes of two binder systems (PVDF–NMP and CMC/SBR–water). Pressure and temperature variations allow conclusions on governing mass transport resistances inside the electrode coils during postdrying and moisture management. This study provides a basis to

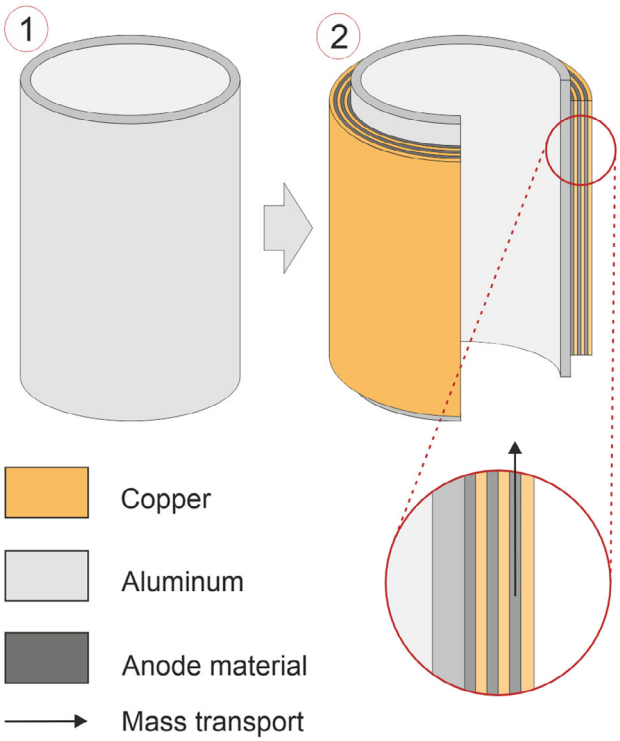

Figure 8. The cylinder (1) is the empty sample holder made of aluminum. The cylinder is perforated with a pattern (not shown) to reduce weight and increase accuracy of the gravimetric measurement data. Schematic (2) illustrates a sample holder loaded with an anode. The cross section shows that several layers of electrode are wound up.

© 2022 The Authors. Energy Technology published by Wiley-VCH GmbH

21944296, 0, Downloaded from https://onlinelibrary.wiley.com/doi/10.1002/ente.202200859 by Karlsruher Inst F. Technologie, Wiley Online Library on [11/10/2022]. See the Terms and Conditions (https://onlinelibrary.wiley.com/terms-and-conditions) on Wiley Online Library for rules of use; OA articles are governed by the applicable Creative Commons License

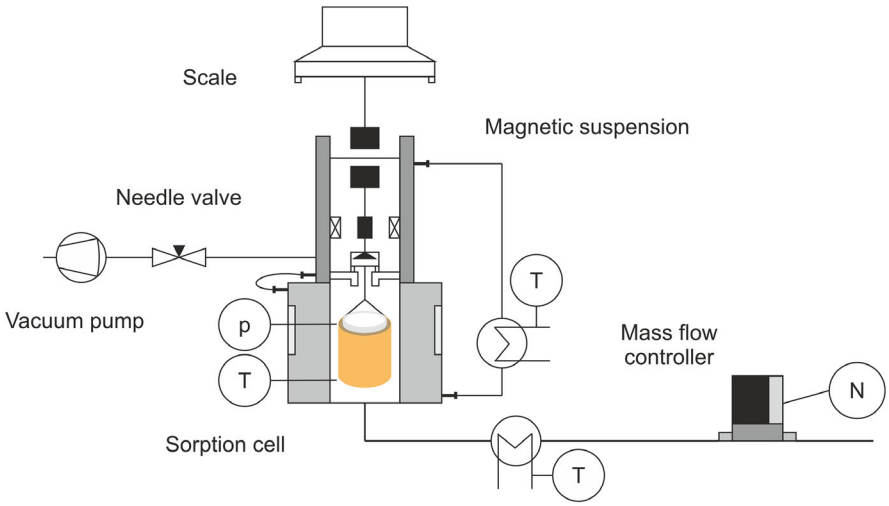

Figure 9. Experimental setup to measure desorption kinetics of laboratory-scale electrode coils at various pressures and temperatures. The continuous flow through the sorption cell ensures constant boundary conditions for the desorption.

fundamentally understand sorption and mass transport phenomena during moisture management and postdrying.

4. Experimental Section

Materials: The CMC/SBR anode consisted of 94 wt% SMG-A graphite (nonspherical, Hitachi Chemical Co. Ltd.), 2 wt% CMC sodium salt binder (CMC MAC500LC, Nippon), 2 wt% SBR binder (Zeon), and 2 wt% carbon black (SuperC65, Imerys). The PVDF-anode consisted of 91.7 wt% SMG-A graphite (spherical, Hitachi Chemical Co. Ltd., Japan), 5.5 wt% polyvinylidene fluoride (PVDF, Solef 5130, Solvay), and 2.8 wt% carbon black (SuperC65, Imerys). The substrate of both electrodes was copper foil.

Samples: The materials were processed into CMC/SBR anodes and PVDF anode sheets by the routines of Keppeler et al. and Jaiser et al, respectively.[31,32] The electrode sheets were cut to size and mounted onto the sample holder, which is illustrated in **Figure 8**.

Figure 8 shows the samples that resemble an electrode coil regarding geometry and diffusion path during the vacuum drying of electrode coils. The electrode sheets were tightly wound around the sample holder (coil) to minimize the gaps between two layers of electrodes. The final layer was fixed with tin solder. However, thin gaps between individual layers may occur and accelerate the mass transport through the electrode coils. One sample for the CMC/SBR anode and one sample for the PVDF anode was used to obtain all experimental data. Therefore, potential gaps between electrode layers would affect every experiment of the respective anode similarly. The coil had a diameter of 4 cm and a length of 10 cm. This geometry ensured a 1D diffusion path along the axial direction of the coil. This setup was used for CMC/SBR anodes as well as for PVDF anodes.

Experimental Setup: A magnetic suspension microbalance combined with a sorption unit[33–35] and vacuum drying setup measures the drying curves of the electrode coil samples (compare **Figure 9**). The magnetic suspension balance couples the weighing unit with the sample without mechanical contact.[14,33] This setup allows the precise conditioning of the measuring cell regarding pressure, relative humidity, and temperature. The sorption unit adjusts the relative humidity in the measuring cell by temperature controlling the solvent evaporator and cell individually. The combination of a needle valve and a mass-flow controller enables the adjustment of the pressure inside the measurement cell while continuously exchanging the gas phase. The pressure settings and respective volume settings are summarized in **Table 1**.

Table 1. Pressure settings for vacuum drying and the respective mass flows that exchange the gas volume in the measuring cell.

Pressure [mbar]	800	400	100	40	20	40[b)]	20[b)]
Volume flux [L min^{-1}]	2.5	2.3	4.2	3.1	1.9	22.6	11.8
Retention time[a)] [s]	25	27	15	20	33	2.8	5.3

[a)]The cells volume is 1.04 L; [b)]High-volume flux option.

Drying Curves: The sorption unit of the setup adjusts repeatable starting conditions for each drying experiment. Samples were predried at 90 °C and maximum power of the vacuum pump ($\approx 10^{-3}$ mbar) until no further change in mass was detectable. Subsequently, the samples were loaded with water to their sorption equilibrium at a relative humidity of 55%. The change from this relative humidity to a continuous flow of dry ($T_{\text{Dew point}} = -65$ °C) initialized postdrying. Table 1 lists the flow conditions inside the cell at each system pressure. High-volume fluxes (Footnote (b) in Table 1) ensure a dry boundary condition even for fast drying experiments, for example, PVDF anode at 80 °C. The system configuration enables high-volume fluxes for 20 and 40 mbar.

Supporting Information

Supporting Information is available from the Wiley Online Library or from the author.

Acknowledgements

The authors acknowledge the financial support of the Federal Ministry of Education and Research (BMBF) within the "ProZell" cluster project "Epic" under the reference number 03XP0295A. This work contributes to the research performed at Center for Electrochemical Energy Storage Ulm-Karlsruhe (CELEST). The authors would also like to thank Sebastian Lukas, Lukas Heckmann, Johannes Dörr, and Felix Hollert for experimental support.

Open Access funding enabled and organized by Projekt DEAL.

© 2022 The Authors. Energy Technology published by Wiley-VCH GmbH

21944296, 0, Downloaded from https://onlinelibrary.wiley.com/doi/10.1002/ente.202200859 by Karlsruher Inst F. Technologie, Wiley Online Library on [11/10/2022]. See the Terms and Conditions (https://onlinelibrary.wiley.com/terms-and-conditions) on Wiley Online Library for rules of use; OA articles are governed by the applicable Creative Commons License

Conflict of Interest

The authors declare no conflict of interest.

Data Availability Statement

The data that support the findings of this study are available from the corresponding author upon reasonable request.

Keywords

electrode production, Li-ion batteries, mass transport, moisture management, postdrying sorption

Received: July 29, 2022
Revised: September 5, 2022
Published online:

[1] J. Kaiser, V. Wenzel, H. Nirschl, B. Bitsch, N. Willenbacher, M. Baunach, M. Schmitt, S. Jaiser, P. Scharfer, W. Schabel, *Chem. Ing. Tech.* **2014**, *86*, 695.
[2] A. Kwade, W. Haselrieder, R. Leithoff, A. Modlinger, F. Dietrich, K. Droeder, *Nat. Energy* **2018**, *3*, 290.
[3] S. N. Bryntesen, A. H. Strømman, I. Tolstorebrov, P. R. Shearing, J. J. Lamb, O. Stokke Burheim, *Energies* **2021**, *14*, 1406.
[4] W. B. Hawley, J. Li, *J. Energy Storage* **2019**, *25*, 100862.
[5] F. Huttner, W. Haselrieder, A. Kwade, *Energy Technol.* **2020**, *8*, 1900245.
[6] F. Huttner, A. Marth, J. C. Eser, T. Heckmann, J. Mohacsi, J. K. Mayer, P. Scharfer, W. Schabel, A. Kwade, *Batteries Supercaps* **2021**, *4*, 1499.
[7] J. Kumberg, W. Bauer, J. Schmatz, R. Diehm, M. Tönsmann, M. Müller, K. Ly, P. Scharfer, W. Schabel, *Energy Technol.* **2021**, *9*, 2100367.
[8] J. K. Mayer, L. Almar, E. Asylbekov, W. Haselrieder, A. Kwade, A. Weber, H. Nirschl, *Energy Technol.* **2020**, *8*, 1900161.
[9] M. Stich, N. Pandey, A. Bund, *J. Power Sources* **2017**, *364*, 84.
[10] A. R. Schuer, M. Kuenzel, S. Yang, M. Kosfeld, F. Mueller, S. Passerini, D. Bresser, *J. Power Sources* **2022**, *525*, 231111.
[11] J.-H. Schünemann, H. Dreger, H. Bockholt, A. Kwade, *ECS Trans.* **2016**, *73*, 153.
[12] J. C. Eser, B. Deichmann, T. Wirsching, L. Merklein, M. Müller, P. Scharfer, W. Schabel, *Drying Technol.* **2020**, *40*, 1130.
[13] J. C. Eser, B. Deichmann, T. Wirsching, P. G. Weidler, P. Scharfer, W. Schabel, *Langmuir* **2020**, *36*, 6193.
[14] J. C. Eser, T. Wirsching, P. G. Weidler, A. Altvater, T. Börnhorst, J. Kumberg, G. Schöne, M. Müller, P. Scharfer, W. Schabel, *Energy Technol.* **2020**, *8*, 1801162.
[15] F. Huttner, A. Diener, T. Heckmann, J. C. Eser, T. Abali, J. K. Mayer, P. Scharfer, W. Schabel, A. Kwade, *J. Electrochem. Soc.* **2021**, *168*, 90539.
[16] D. S. Scott, F. A. L. Dullien, *AIChE J.* **1962**, *8*, 113.
[17] J. Li, C. Daniel, S. J. An, D. Wood, *MRS Adv.* **2016**, *1*, 1029.
[18] J. Sicklinger, M. Metzger, H. Beyer, D. Pritzl, H. A. Gasteiger, *J. Electrochem. Soc.* **2019**, *166*, A2322.
[19] M. Wood, J. Li, R. E. Ruther, Z. Du, E. C. Self, H. M. Meyer, C. Daniel, I. Belharouak, D. L. Wood, *Energy Storage Mater.* **2020**, *24*, 188.
[20] C. Busà, M. Belekoukia, M. J. Loveridge, *Electrochim. Acta* **2021**, *366*, 137358.
[21] C.-C. Li, C.-A. Chen, M.-F. Chen, *Ceram. Int.* **2017**, *43*, S765.
[22] L. Neidhart, K. Fröhlich, N. Eshraghi, D. Cupid, F. Winter, M. Jahn, *Nanomaterials* **2022**, *12*, 317.
[23] R. Sahore, D. L. Wood, A. Kukay, K. M. Grady, J. Li, I. Belharouak, *ACS Sustainable Chem. Eng.* **2020**, *8*, 3162.
[24] R. B. Evans, G. M. Watson, E. A. Mason, *J. Chem. Phys.* **1961**, *35*, 2076.
[25] W. G. Pollard, R. D. Present, *Phys. Rev.* **1948**, *73*, 762.
[26] M. Tassopoulos, D. E. Rosner, *Chem. Eng. Sci.* **1992**, *47*, 421.
[27] E. N. Fuller, P. D. Schettler, J. C. Giddings, *Ind. Eng. Chem.* **1966**, *58*, 18.
[28] J. Kärger, D. M. Ruthven, T. N. Theodōru, *Diffusion in Nanoporous Materials*, Wiley-VCH-Verl., Weinheim **2012**.
[29] D. Oehler, P. Seegert, T. Wetzel, *Energy Technol.* **2020**, *9*, 2000574.
[30] W. Bauer, D. Nötzel, V. Wenzel, H. Nirschl, *J. Power Sources* **2015**, *288*, 359.
[31] S. Jaiser, J. Kumberg, J. Klaver, J. L. Urai, W. Schabel, J. Schmatz, P. Scharfer, *J. Power Sources* **2017**, *345*, 97.
[32] M. Keppeler, S. Roessler, W. Braunwarth, *Energy Technol.* **2020**, *8*, 2000183.
[33] W. Schabel, I. Mamaliga, M. Kind, *Chem. Ing. Tech.* **2003**, *75*, 36.
[34] W. Schabel, P. Scharfer, M. Kind, I. Mamaliga, *Chem. Eng. Sci.* **2007**, *62*, 2254.
[35] I. Mamaliga, W. Schabel, M. Kind, *Chem. Eng. Process. Process Intensif.* **2004**, *43*, 753.

© 2022 The Authors. Energy Technology published by Wiley-VCH GmbH

21944296, 0, Downloaded from https://onlinelibrary.wiley.com/doi/10.1002/ente.202200859 by Karlsruher Inst F. Technologie, Wiley Online Library on [11/10/2022]. See the Terms and Conditions (https://onlinelibrary.wiley.com/terms-and-conditions) on Wiley Online Library for rules of use; OA articles are governed by the applicable Creative Commons License